Monitoring blood flow alterations in the Tg2576 mouse model of Alzheimer's disease by in vivo magnetic resonance angiography at 17.6 T

Kara, F.; Dongen, E.S. van; Schliebs, R.; Buchem, M.A. van; Groot, H.J.M. de; Alia, A.

NeuroImage 60 (2012) 958–966

Contents lists available at SciVerse ScienceDirect

NeuroImage

journal homepage: www.elsevier.com/locate/ynimg

Monitoring blood flow alterations in the Tg2576 mouse model of Alzheimer's disease by *in vivo* magnetic resonance angiography at 17.6 T

F. Kara [a], E.S. van Dongen [a], R. Schliebs [b], M.A. van Buchem [c], H.J.M. de Groot [a], A. Alia [a,c,*]

[a] SSNMR, Leiden Institute of Chemistry, Gorlaeus Laboratoria, Einsteinweg 55, P.O. Box 9502, 2300 RA Leiden, The Netherlands
[b] Department of Neurochemistry, Paul Flechsig Institute for Brain Research, University of Leipzig, Jahnallee 59, D-04109 Leipzig, Germany
[c] Department of Radiology, Leiden University Medical Center, Albinusdreef 2, 2333 ZA Leiden, The Netherlands

ARTICLE INFO

Article history:
Received 9 September 2011
Revised 16 November 2011
Accepted 18 December 2011
Available online 29 December 2011

Keywords:
Alzheimer's disease
Magnetic field strength
Magnetic resonance angiography
Transgenic mouse
Vascular alterations

ABSTRACT

Many neurodegenerative diseases including Alzheimer's disease are linked to abnormalities in the vascular system. In AD, the deposition of amyloid β (Aβ) peptide in the cerebral vessel walls, known as cerebral amyloid angiopathy (CAA) is frequently observed, leading to blood flow abnormalities. Visualization of the changes in vascular structure is important for early diagnosis and treatment. Blood vessels can be imaged non-invasively by magnetic resonance angiography (MRA). In this study we optimized high resolution MRA at 17.6 T to longitudinally monitor morphological changes in cerebral arteries in a Tg2576 mouse model, a widely used model of AD. Our results at 17.6 T show that MRA significantly benefits from the ultra-high magnetic field strength especially to visualize smaller vessels. Visual and quantitative analysis of MRA results revealed severe blood flow defects in large and medium sized arteries in Tg2576 mice. In particular blood flow defects were observed in the middle cerebral artery (MCA) and in the anterior communicating artery (AComA) in Tg2576 mice. Histological data show that Aβ levels in the vessel wall may be responsible for impaired cerebral blood flow, thereby contributing to the early progression of AD. To our knowledge this is the first ultra-high field MRA study monitoring blood flow alterations longitudinally in living Tg2576 mice, consequently providing a powerful tool to test new therapeutic intervention related to CAA in a mouse model of AD.

Introduction

Alzheimer's disease (AD) is the most common form of dementia with no effective treatment or definitive ante mortem diagnostic test. The neuropathologic features of AD include the occurrence of amyloid β (Aβ)-containing plaques, neurofibrillary tangles, decreased synaptic density, and loss of neurons (Duyckaerts et al., 2008; Schliebs and Arendt, 2011). In addition, cerebrovascular abnormalities coexist with these pathological features of AD. In particular, the deposition of amyloid in the cerebral vessel walls, known as cerebral amyloid angiopathy (CAA) is frequently observed, leading to blood flow abnormalities in AD (Biffi and Greenberg, 2011; Kumar-Singh, 2008). Small to medium-sized arteries and arterioles are the most frequently affected vessels by CAA in AD (Ghiso and Frangione, 2001; Pezzini et al., 2009; Revesz et al., 2002). Though CAA is very common in the advanced stages of AD, its contribution to the onset and progression of AD is unknown.

The evidence for blood flow disturbance in AD comes mainly from postmortem studies (Ellis et al., 1996; Pfeifer et al., 2002). Yamada (2002) has reported that among AD patients (n = 82), the frequency of CAA was 87%, whereas the frequency of CAA in elderly non-AD (n = 119) patients was only 35%. CAA of Aβ type, defined by the accumulation of β-amyloid peptide (Aβ) in cerebral vessels, is the most common form of CAA in elderly population as well as patients with AD (Yamada, 2000). Currently *in vivo* diagnosis of CAA relies on detecting indirect symptoms such as hemorrhage, microbleeding and abnormal vascular reactivity (Biffi and Greenberg, 2011; Smith et al., 2008). Although positron emission tomography in combination with Pittsburg compound, has been shown to detect CAA in AD patients (Biffi and Greenberg, 2011), the need to use ionizing radiation for PET and unspecificity of Pittsburg compound for distinguishing between parenchymal and vascular Aβ plaques impede the use of this method on a large scale.

Transgenic mouse models of AD have been used to understand how CAA related blood flow abnormalities contribute to the onset and progression of AD (Hawkes et al., 2011; Herzig et al., 2004; Merlini et al., 2011; Meyer et al., 2008; Nishitsuji et al., 2007; Poduslo et al., 2011; Thal et al., 2009). *Ex vivo* studies in human and in transgenic mouse models have reported similar observations regarding CAA related morphological changes in vascular structures leading to blood flow defects in AD. Recently, an upregulation of the angiogenic vascular endothelial growth factor (VEGF) by cortical vascular endothelial cells in 21-month-old transgenic Tg2576 mice has

* Corresponding author at: Leiden Institute of Chemistry, Gorlaeus Laboratoria, Einsteinweg 55, P.O. Box 9502, 2300 RA Leiden, The Netherlands. Fax: +31 715274623.
E-mail address: a.alia@chem.leidenuniv.nl (A. Alia).

1053-8119/$ – see front matter © 2011 Elsevier Inc. All rights reserved.
doi:10.1016/j.neuroimage.2011.12.055

been observed suggesting a role of VEGF in formation of vascular Aβ and mediating CAA (Bürger et al., 2009, 2010). However, direct *in vivo* methods to probe blood flow disturbance during AD in mice are highly challenging. *In vivo* magnetic resonance (MR) techniques currently used for AD evaluations in humans and mouse models of AD are in a state of progression with continued reassessment for enhanced diagnostic accuracy (Braakman et al., 2006; Kantarci and Jack, 2004). Non-invasive MR imaging techniques, such as *in vivo* magnetic resonance angiography (MRA), have shown great potential to study blood flow defects in APP23 and APP/PS1 mouse models of AD (Beckmann et al., 2003, 2011; El Tannir El Tayara et al., 2010). In this technique shortening of the effective longitudinal relaxation time (T1) of moving blood provides the vessel contrast with stationary tissue (Hu and Norris, 2004). While global architecture of the cerebral vasculature could be detected in both APP23 and APP/PS1 mice by *in vivo* MRA at 4.7 T magnetic field strength, further improvement in visualization is desirable, especially for detection of small arteries with low blood flow rate. The small size of the mouse brain has considerable limitations for MRA in visualizing cerebral vasculature with high spatial resolution and signal-to-noise ratio at low magnetic field strength (≥4.7 T). The T1 relaxation time of tissue increases with the field strength (van de Ven et al., 2007). Increased T1 relaxation time and high magnetization at higher fields provides improved signal-to-noise ratio and higher vessel-to-tissue contrast that may contribute to the improved quality of MRA (Fushimi et al., 2006). Therefore, moving to high (such as 9.4 T) or ultra-high (such as 17.6 T) magnetic field can significantly improve visualization of cerebral vasculature and blood flow abnormalities in mouse models of AD as well as for other neurodegenerative diseases. Tg2576 is one of the most widely used transgenic mouse models of AD (Hsiao et al., 1996). In this model accumulation of Aβ in cerebral vessels starts between 9 and 12 months of age and severity of CAA increases during aging (Christie et al., 2001; Domnitz et al., 2005; Holtzman et al., 2000; Kumar-Singh et al., 2005; Shin et al., 2007). Reports on MRA for this mouse model are lacking. In addition, the *in vivo* relationship between amyloid plaque deposition in brain tissue and its correlation with blood flow alterations is not clear.

The aim of this study was to: (1) achieve improved visualization of cerebral vasculature by optimizing and applying *in vivo* MRA at 17.6 T magnetic field strength; (2) detect AD related blood flow defects in cerebral arties in Tg2576 mice; and (3) longitudinally follow, *in vivo* amyloid plaque deposition in brain tissue and its correlation with CAA related morphological changes in cerebral arteries and blood flow alterations in the same Tg2576 mice with age.

Materials and methods

Mice

In this study transgenic Tg2576 mice developed and described by Hsiao et al. (1996) were used as model of AD. The mice contained as transgene the human amyloid precursor protein (APP695) with the Swedish double mutation (K670N, M671L) under control of a hamster prion protein promoter (Hsiao et al., 1996). Three founder mice were kindly provided by Dr Karen Hsiao Ashe (University of Minnesota) and used for further breeding. Mice heterozygous for the transgene and wild-type littermates were on a C57BL/6 x SJL background. At the age of four weeks transgeneity was identified by polymerase chain reaction of tail DNA as described elsewhere (Hsiao et al., 1996). The N2 generation mice of both genders were studied at the ages of 12–18 months. Age-matched non-transgenic littermates served as controls. In addition, C57BL/6 mice (9 months old) were used for optimization studies. All of the animal experiments were approved by the institutional animal care and animal use committee of the University of Leiden in accordance with the NIH Guide for the Care and Use of Laboratory Animals.

Histology

Histological analyses were performed to assess amyloid deposits and CAA in Tg2576 mice by following the procedure as described previously (Braakman et al., 2006). The mice were decapitated and brains were fixed in 4% buffered paraformaldehyde (Zinc Formal-Fixx, ThermoShandon, UK) for 48 h. Following fixation brains were dehydrated and embedded in paraffin. Subsequently coronal sections (5 μm thick) were carefully cut using a vibratome while maintaining as much as possible the same spatial orientation of the mouse brain as in the μMRI experiments. To detect Aβ, brain sections were subjected to immunohistochemistry using anti-Aβ (6E10), anti-Aβ40 (BC40) or anti-Aβ42 (BC42). Immunolabeling was visualized by using the ABC kit (Vectastain) according to the manufacturer's instructions.

Magnetic resonance microimaging (μMRI)

All measurements were conducted on a vertical wide bore 9.4 T or 17.6 T Bruker spectrometer with a 1000 mTm^{-1} actively shielded imaging gradient insert (Bruker Biospin GmbH, Germany). A birdcage radio-frequency (RF) coil (inner diameter 2 cm) was used. The system was interfaced to a Linux PC running XWinNMR 3.2 and Paravision 5.0 (Bruker Biospin GmbH, Germany) software.

All *in vivo* MR imaging studies were conducted as previously described (Braakman et al., 2006). Before MR imaging, the mice were anesthetized with 2% isoflurane (Forene, Abott, UK), in air (0.3 l/min) and oxygen (0.3 l/min). During scanning the isoflurane concentration was maintained between 1 and 1.5% to keep the breathing of the animal at a constant rate of ~50 breaths per minute. Animals were placed in a birdcage RF coil with a special mouse head mask, which was used to administer the anesthetic gas during MR experiments. A respiration sensor, connected to a respiration unit, was placed on the abdomen of the mouse, to monitor it's respiration rate during the MR imaging. The respiration unit was connected to a computer having Bio-SAM respiration monitoring software (Bruker Biospin, Germany). The body temperature of the mouse was kept constant by pumping warm water through the gradient system. The rectal body temperature of the mouse during scanning was measured to be 35 ± 1 °C.

T_2-weighted MR images were acquired with a multislice rapid acquisition with relaxation enhancement (RARE) (Hennig et al., 1986) sequence at 9.4 T. Coronal images were obtained with a slice thickness of 0.5 mm. A resolution of 78 × 78 μm was achieved within an acquisition time of ~25 min. The imaging parameters used for the RARE sequence were: TE = 11.6 ms (effective TE = 23.33 ms); TR = 6 s; FA = 90°, averages = 4, RARE factor (echo train length) = 4; FOV = 2.00 × 2.00 cm^2 and image matrix = 256 × 256. Quantification of Aβ plaque load in MR images was done as described earlier (Braakman et al., 2006).

Magnetic resonance angiography (MRA)

Time-of-flight (TOF) angiograms were obtained using a three-dimensional (3D) gradient-echo sequence. To find the optimum combination of parameters for TOF-MRA at 17.6 T, variable flip angle (FA) and repetition time (TR) parameters of the 3D time-of-flight (TOF) gradient echo sequence were systematically varied to obtain the best image quality in a reasonable imaging time. The following parameters were used: Echo time (TE) = 1.86 ms; field-of-view (FOV) = 15 × 15 × 15 mm; matrix size = 128 × 128 × 128; FA = 10°, 15°, 20°, 30°, 40° or 50°; TR = 15, 20, 30, or 40 ms.

Optimized scan parameters used to acquire high-resolution 3D-MRA of transgenic mice and non-transgenic littermates were as follows: TE = 1.86 ms; FOV = 17 × 17 × 17 mm; matrix size = 256 × 192 × 192; FA = 20°; and TR = 20 ms. All data were zero-filled to 256 × 256 × 256.

Three-dimensional TOF MRA was compared at 9.4 T and 17.6 T. All imaging parameters were kept the same at both magnetic fields. Imaging parameters were TE = 1.86 ms; TR = 20 ms; FA = 20°. All data (matrix size 256×192×192) were zero-filled to 256×256×256. The total acquisition time of 3D-TOF was ~9 min. Three-dimensional view was obtained by generating maximum-intensity projections (MIP) using Paravision 5 software (Bruker Biospin, GmbH, Germany).

Identification of cerebral arteries was performed by inspecting the angiograms under various angles and comparing the vessels to the anatomical atlas of Dorr et al. (Dorr et al., 2007) and previous reports in the literature (Beckmann et al., 1999; El Tannir El Tayara et al., 2010; Okuyama et al., 2004; Reese et al., 1999; Schambach et al., 2009).

Image analysis and quantification

The severity of the vascular abnormalities in Tg2576 mice and non-transgenic control mice was evaluated by visual assessment as well as by a semi-quantitative analysis.

Visual assessment of MCA was based on the pointing system as described earlier (El Tannir El Tayara et al., 2010). According to this system, blood flow abnormalities were graded on the basis of the number and extents of signal voids detected on the MR angiograms. A flow disturbance was counted when a decrease of the signal was visible on the scan, but the signal intensity at the level of the artery did not yet reach background level. A void was counted when the signal intensity at the level of the artery reaches the background level. Furthermore a distinction was made between a small void and an extended void. The grades were defined as follows: (1) flow disturbance visible, but the artery shape was unaltered; (2) one or two small signal voids: a small signal void was defined as a void with a maximum length of twice the diameter of the artery; (3) more than 2 small signal voids; (4) one extended signal void: an extended void was defined as a void with a length larger than twice the diameter of the artery; (5) a combination of small and extended voids; and (6) artery was partially or completely missing.

For the semi-quantitative method, the average contrast-to-noise ratio (CNR) and signal-to-noise ratio (SNR) were calculated from the coronal slices (n = 5–9) of the MRA data set. Three regions of interest (ROI) were selected in each slice: (1) an ROI manually delineated in the vessel contour on cross-sectional slices (ROI); (2) an ROI of the background brain tissue without vessels (BG); and (3) an ROI of the surrounding air. The average standard deviation of the ROI in surrounding air was defined as noise (σ). The CNR of each region was calculated as: CNR = (sROI-sBG)/σ (air). The SNR was calculated as: SNR = sROI/σ (air). "s" refers to average signal intensity within the selected area. Signal intensity of ROI placed on the vessel was calculated above a threshold value corresponding to s(BG) + [0.1x s(BG)].

The means and standard deviations of each region were calculated. The statistical comparisons were made by pooling all slice measurements from all the datasets in a given sample group and performing one-tailed and/or two-tailed Student's *t*-test. Statistical significance was assigned for P values < 0.05.

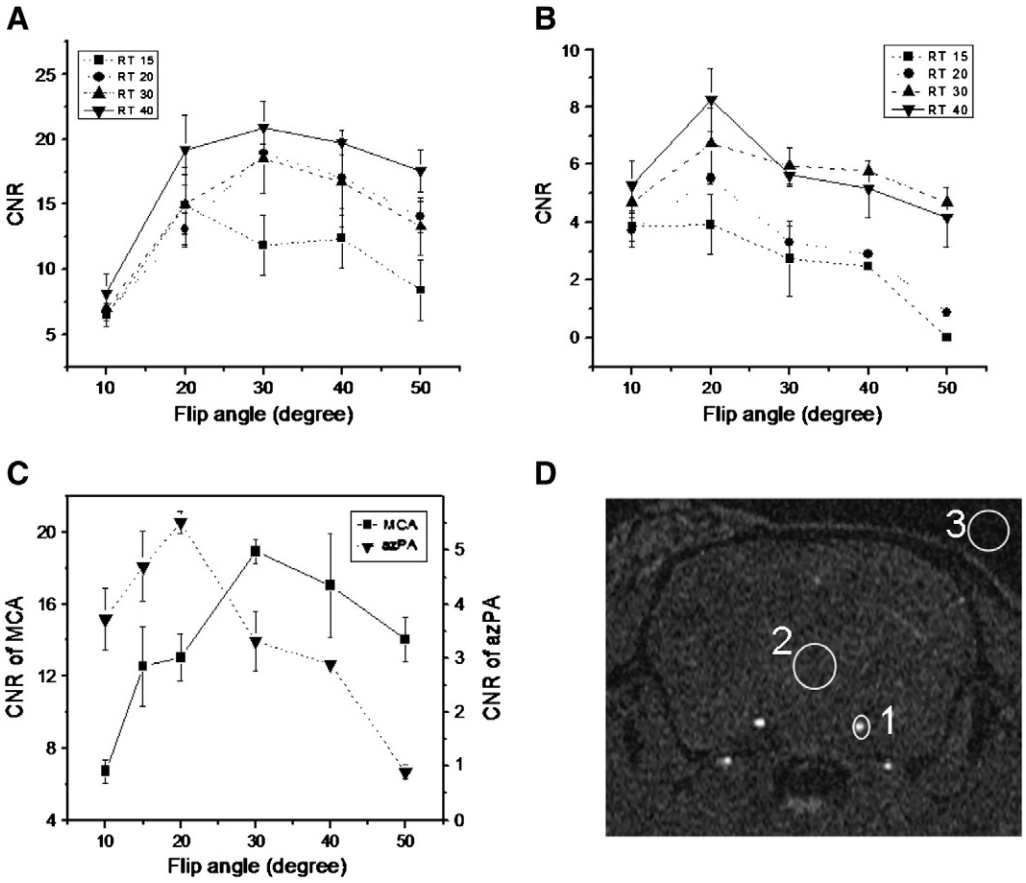

Fig. 1. Optimization of 3D TOF-MRA at 17.6 T magnetic field strength. (A) The effect of varying the radiofrequency pulse flip angle (FA) and inflow time (repetition time, TR) was evaluated on contrast to noise ratio (CNR) of middle cerebral artery (MCA) (A) and azygos pericallosal artery (azPA) (B). The effect of varying the FA on the CNR of MCA and azPA measured at a constant TR of 20 ms (C). Vessels having higher blood flow such as MCA were better visualized at higher FA (30°), however smaller vessels such as azPA having low blood flow were better visualized at smaller FA (15°–20°). (D) The slice of 3D data set indicating the region of interest for which CNR evaluation was performed (1 = vessel; 2 = background brain tissue; 3 = surrounding air). The optimization was performed on three mice, with nearly identical results. For clarity, the plots are from a single specimen. The values are the mean ± SD (error bars) over five slices.

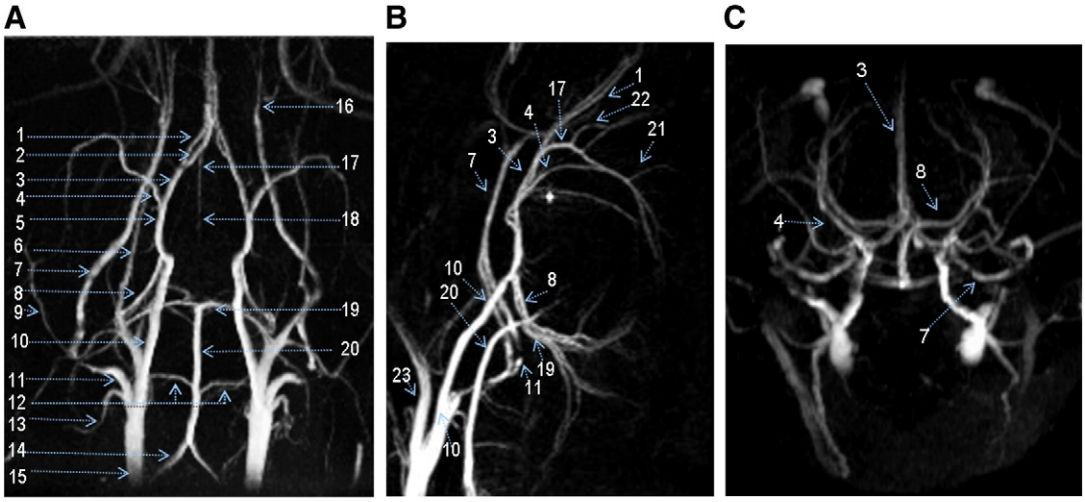

Fig. 2. Coronal (A), sagittal (B) and transverse (C) projection of high-resolution MIPs of a 3D-TOF angiogram of a mouse cerebrovascular system revealing arterial anatomy at 17.6 T magnet field strength. The following arteries were clearly identified: (1) Olfactory artery (OlfA); (2) Anterior communicating artery (AComA); (3) Anterior cerebral artery (ACA); (4) Middle cerebral artery (MCA); (5) & (10) Internal carotid artery (ICA); (6) Facial artery (external Maxillary artery);(7) Palatine portion of pterygopalatine (PPP); (8) Posterior cerebral artery (PCA); (9) Maxillary artery; (11) Pterygo portion of pterygopalatine; (12) Caudal cellebellar artery;(13) A branch of common carotid artery; (14) Vertebral artery (VA); (15) Common carotid artery (CCA); (16) Ophthalmic artery; (17) Anterior azygos cerebral artery (azACA); (18) Azygos pericallosal artery (azPA); (19) Superior cerebellar artery (SCA); (20) Basilar artery (BA); (21) Middle internal frontal artery; (22) Anterior internal frontal artery; and (23) External carotid artery (ECA).

Results and discussion

Optimization of MRA at 17.6 T

The 3D TOF MRA sequence was optimized at 17.6 T to visualize cerebral arteries in living mouse. To find the optimum combination of parameters for TOF MRA at 17.6 T, radiofrequency pulse repetition time (TR) and pulse flip angle (FA) were steadily varied. Fig. 1 shows the effect of varying FA and TR on contrast to noise ratio (CNR) of MCA (Fig. 1A) and azygos pericallosal artery (azPA) (Fig. 1B). As is clear from this figure, MCA which is one of the large vessels with relatively high blood flow (Dorr et al., 2007) has excellent visibility at all combination of FA (20°–50°) and TR (15–40 ms). However small vessels such as azPA are better delineated at smaller FA (20°). While a longer TR offers greater CNR, the TR of 20 ms had been chosen as optimum to obtain reasonable resolution in a relatively short scan time for subsequent measurements. The relationship between CNR and FA (10°–50°) at constant TR (20 ms) of MCA and azPA is shown in Fig. 1C. A representative slice of 3D data set of MRA showing region of interest used for estimation of CNR of vessels with respect to background brain tissue and surrounding air is shown in Fig. 1D.

Fig. 2 depicts a high resolution MRA of a 14-months-old wild-type mouse along the coronal (A) and sagittal (B) and transverse (C)

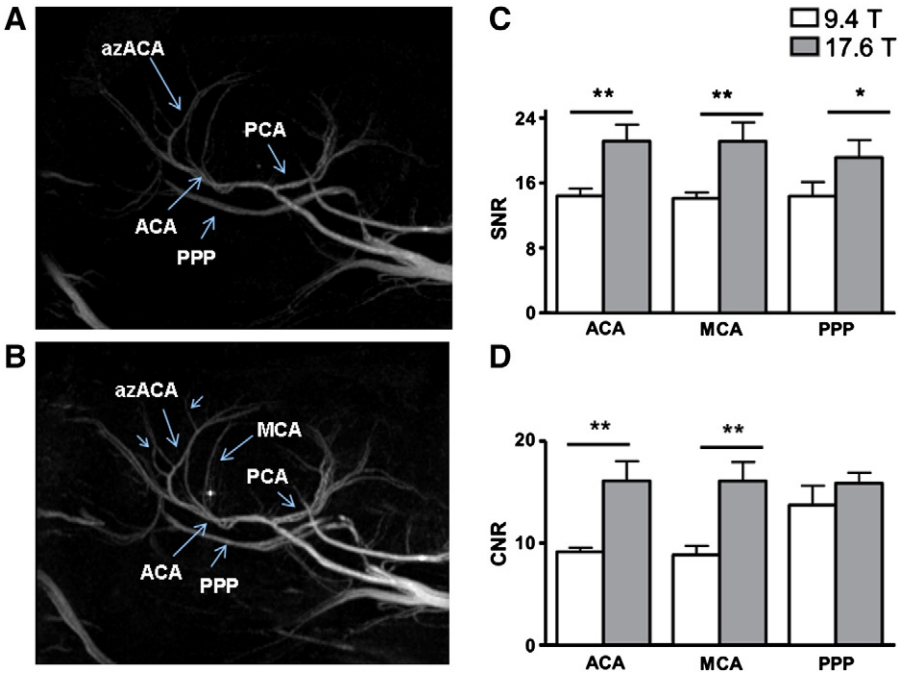

Fig. 3. Angiogram in sagittal view of same 9-month-old wild-type mouse imaged at 9.4 T (A) and 17.6 T (B) magnetic field strengths. Arrows indicate vascular branches, which are better resolved at 17.6 T as compared to 9.4 T. Comparison of SNR (C) and CNR (D) of ACA, MCA and PPP vessels estimated at 9.4 T and 17.6 T. Both CNR and SNR in all three vessels were higher at 17.6 T as compared to 9.4 T. Values are expressed as mean ± SD (error bars). Two-tail student *T* test, *P<0.05, **P<0.01, n = 3.

directions acquired in 9 min using optimized sequence parameters at 17.6 T. Many small and medium size vessels were nicely delineated at 17.6 T within this short scan time.

Field dependence

Fig. 3 compares the angiogram of vascular system of the same wild-type mouse imaged at 9.4 T and 17.6 T. In general MRA at 17.6 T revealed enhanced visualization of vessels compared to the data collected in a field of 9.4 T, especially for small vessels. For example, branches of anterior azygos cerebral artery (azACA) are better resolved at 17.6 T as compared to 9.4 T. Figs. 3C and D summarize the effect of field strength on CNR (a) and SNR (b) of vessels including MCA, anterior cerebral artery (ACA) and palatine portion of pterygopalatine (PPP). The calculated SNR (Fig. 3C) of all three vessels are significantly higher at 17.6 T as compared to 9.4 T. The SNR of MCA, ACA and PPP were ~50%, ~47% and ~33% higher at 17.6 T than at 9.4 T, respectively. MCA and ACA also showed significantly higher CNR (~70–80%) at 17.6 T than at 9.4 T (Fig. 3D). The superior contrast at 17.6 T could be attributed to longer T1 of background tissue as well as greater magnetization of inflowing blood (Howles et al., 2009). The longer T1s of tissues provide better background suppression, which allows improved visualization of smaller distal vessels with MRA. The observed increase in SNR was less than expected for the higher field of 17.6 T. This could be due to increased susceptibility effects and larger field inhomogeneity at higher magnetic field. Since SNR is inversely proportional to the square root of T1, longer T1 at higher field also has an inverse effect on SNR (Dydak and Schar, 2006). Nevertheless the substantial increase of vessel SNR at 17.6 T is offering the possibility to either increase the spatial resolution or to shorten scan times for future mouse MRA studies.

Evaluation of vascular alterations in control and Tg2576 mice with age

To evaluate and compare the *in vivo* vascular alterations in control and Tg2576 mice and to follow changes over time, we applied high resolution MRA at 17.6 T. In general blood flow alterations detected on TOF-angiograms were more frequent in Tg2576 mice as compared to control mice. In particular, the overall decrease in the brightness of arteries and alterations such as flow voids and vessel signal loss were more visible in Tg2576 mice as compared to control mice. Fig. 4 (A and B) shows representative angiograms of two 18-month-old Tg2576 mice. The numbers on the angiogram indicate the appointed score to the level of severity of alterations. The higher the score, the more severe the alteration was. For example, a flow disturbance without apparent change in vessel shape is visible in AComA (score 1 in Fig. 4A); A small signal void was observed at the origin of AComA (score 2 in Fig. 4B); More than two small voids in the same artery were observed in MCA on both sides (score 3 in Fig. 4B); An extended void can be seen in the small branch of common carotid artery (CCA) on both sides (score 4 in Fig. 4A); A combination of an extended void and several small signal voids was observed in the small branches of carotid artery on both sides (score 5 in Fig. 4B). Signal was no longer visible for the pterygo portion of the pterygopalatine artery (score 6 in Figs. 4A and B). Fig. 4C shows the enlarge view of these alterations.

In general, MCA was one of the most altered vessels on TOF-angiogram of Tg2576 mice. A comparison of the alteration mean scores in MCA in Tg2576 and control mice with age is shown in Fig. 4D. The changes in MCA alteration score in control and Tg2576 mice were insignificant at the age of 14 and 16 months while became significantly higher (~57%) at the age of 18 months in Tg2576 mice as compared to the control mice (Fig. 4D). The abnormalities in MCA in Tg2576 mice, detected by MRA in this study, are consistent with in vivo cerebral blood flow alterations observed in MCA in human AD patients (Franceschi et al., 1995; Ishibashi et al., 1998). In these patients, stenoses, hypoperfusion and decreased cerebral blood flow have been reported in the MCA.

Fig. 5 (A and B) compares 3D angiogram and its source-slice data set of control and a Tg2576 mouse. Severe decrease of signal intensity can be seen in anterior communicating artery (AComA) in addition to MCA in Tg2576 mouse, but not in control mice. Visibility of alterations in individual slice of MRA data set validates the changes seen in 3D MIP in Tg2576 mice. An age-dependent evaluation of contrast-to-noise ratio (CNR) changes was performed in the source data images for every mouse for MCA and AComA (Figs. 5C and D). In both control and Tg2576 mice, an overall decrease in vessel CNR was observed with age. However, decrease in CNR was more significant in Tg2576 mice than in control mice especially at the age of 18 months (Figs. 5C and D). A 3D representation of age-dependent changes seen in AComA in control and Tg2576 mice is shown in Fig. 5E. The arteries such as ACA, and olfactory artery (OlfA) in Tg2576 mice also showed a decreasing trend in CNR as compared with control mice, although this decrease did not reach statistical significance (supplementary Fig. S1). Age-dependent increase in blood flow defects were also observed in a small branch of common carotid artery in Tg2576 mice (supplementary Fig. S2).

Thus, our results show that blood flow alterations in Tg2576 mice can be very well detected with MRA at 17.6 T and can be followed longitudinally in the same mice with age. The blood flow abnormalities detected by MRA in the Tg2576 mice are consistent with cerebrovascular abnormalities reported in human AD patients (Franceschi et al., 1995; Ishibashi et al., 1998). These findings suggest that Tg2576 is

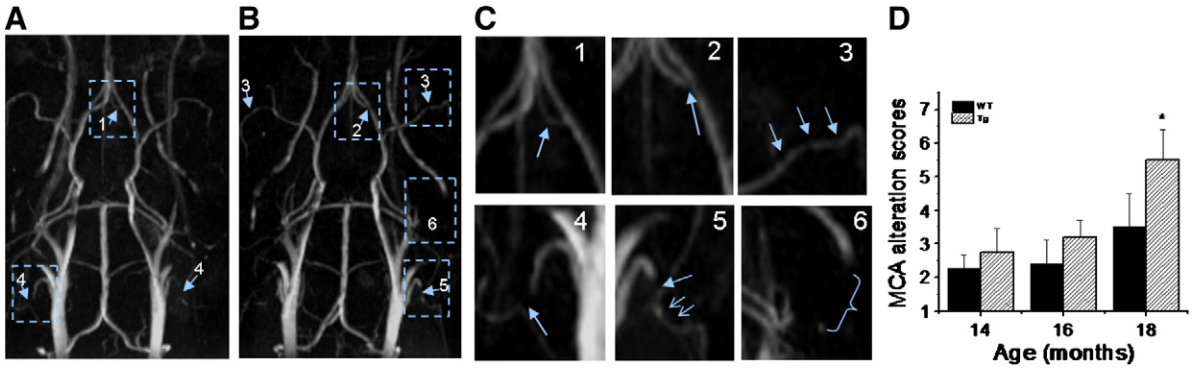

Fig. 4. (A, B) Angiograms collected at 17.6 T magnet of 18-month-old transgenic mice showing various level of severities of morphological changes appointed in 3D MIP. The number indicates the appointed score to the level of severity of alterations. For example: 1 = a *flow disturbance* (as seen in AComA in image A); 2 = a *small signal void* (as observed at the origin of AComA in image B); 3 = *more than two small voids* in same artery (as observed on the MCA on both sides in image B); 4 = an *extended void* (as observed in the external carotid artery on both sides in image A); 5 = a combination of *an extended void and several small signal voids* (as observed in the external carotid artery on both sides in image B); 6 = *the signal is no longer visible* (as shown at the pterygo portion of the pterygopalatine artery in image A and B). The enlarge view of alterations is shown in C). (D) MCA alteration mean score in control and Tg2576 mice with age. Values are mean ± SE (error bars); one-tail student *T* test; *P<0.05; n = 4.

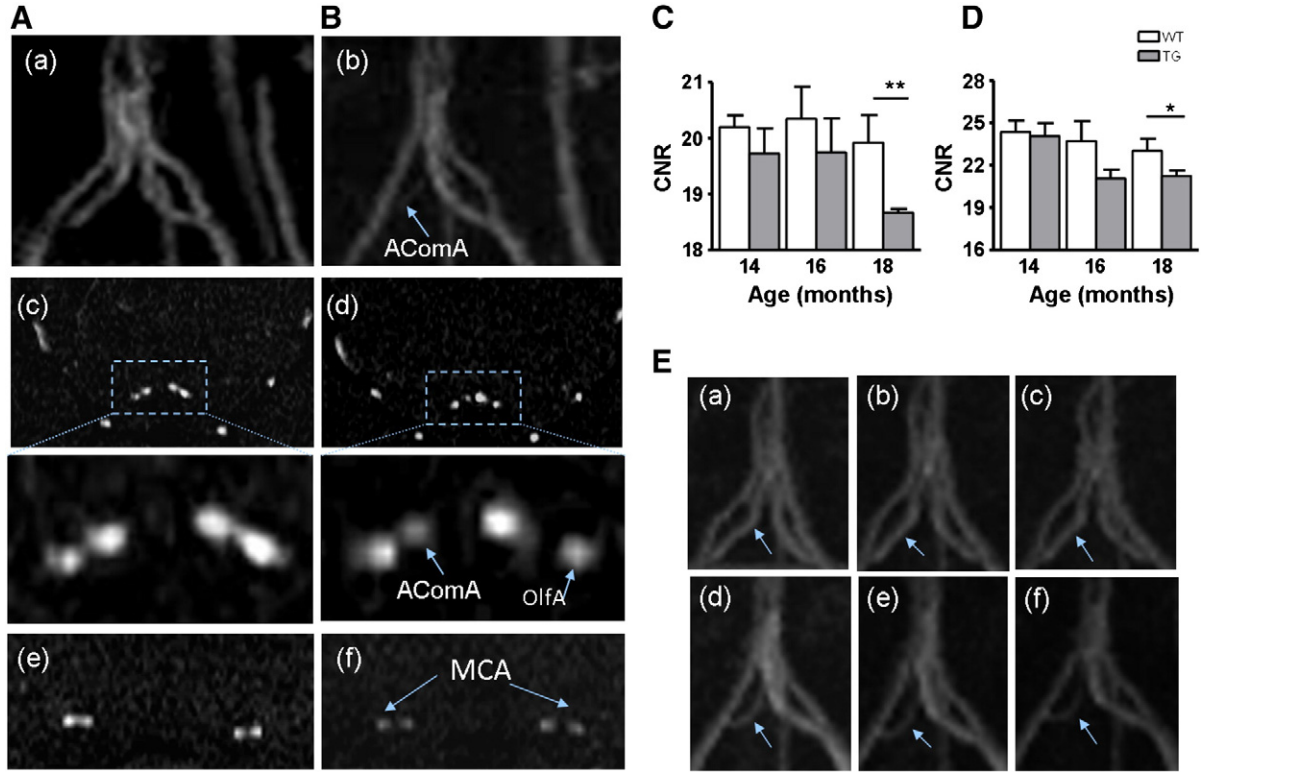

Fig. 5. Representative MIP images and source-slice data set of an 18-month-old control (A) and Tg2576 mouse (B). Tg2576 mouse exhibited severe blood flow alteration at one of the AComA as depicted by arrow (b) which was not visible in control mice (a). The slices of 3D angio data collected at 17.6 T magnet indicating the regions used for the signal intensity evaluation for control (c, e) and Tg2576 (d, f) mice. Severe decrease of signal intensity was observed in AComA and MCA in Tg2576 mice. **(C)** Age-dependent changes in contrast-to-noise ratio (CNR) of AComA **(C)** and MCA (D) in control and Tg2576 mice. One-tail student *T* test was used for statistical evaluation. *$P<0.05$ and **$P<0.01$. The number of animals per age is as follows: control mice: age 14th month ($n=8$), 16th month ($n=6$), and 18th month ($n=6$); Tg2576 age 14th month ($n=8$), 16th month ($n=7$), and 18th month ($n=6$). (E) Age-dependent changes in AComA in a control mouse (a–c) and a Tg2576 (d–f) mouse imaged at the age of 14 (a,d); 16 (b, e) and 18 (c, f) months.

a valid mouse model for studying CAA related blood flow abnormalities in vivo. The hypointensities seen in 3D MIP of the mouse brain might be caused by a number of interrelated factors such as changes in vessel morphology (narrowing, compression, partial occlusion etc.) and/or complex blood flow patterns (turbulent flow, reversal, acceleration or very slow blood flow) (Anderson et al., 1990; Beckmann, 2011; El Tannir El Tayara et al., 2010). Any of these factors can lead to loss of signal within cerebral arteries. Beckmann et al. (2003) used the corrosion casts method to identify the underlying structural changes in the cerebrovascular system of APP23 AD mouse and showed that morphological anomalies of the vessel, such as constrictions and/or narrowing, occur at the sites where altered perfusion were detected by MRA (Beckmann et al., 2003). More recently the study of Thal et al. (2009) has signified the association of CAA with cerebral blood flow disturbance seen in MRA in APP23 mice. The blood flow alterations in Tg2576 seen in the present study may be associated with CAA related elevation of Aβ levels in the vessel wall (Domnitz et al., 2005). Fig. 6 shows the angiogram of an 18 month-old wild-type and a Tg2576 mouse, indicating flow disturbance in the branches of the MCA in Tg2576 mice (Figs. 6A–D). Histological staining of Aβ confirmed the presence of CAA in the territory of the pial branches of the MCA of the Tg2576 mouse, but not in the wild-type mouse (Figs. 6E–F), suggesting a causal role of CAA on the blood flow alterations monitored by MRA. In addition, the immunohistochemistry also shows large prevalence of the Aβ40 isoform in cerebral vessel walls of Tg2576 mice, as compared to the Aβ42 isoform (Figs. 7A–C). These results are consistent with previous reports showing that dense plaques and CAA in Tg2576 mice are predominantly composed of Aβ40 (Harigaya et al., 2006; Kumar-Singh et al., 2005) and that Aβ40 could play a role in the cerebrovascular alterations observed in Alzheimer's disease (Han et al., 2008; Niwa et al., 2000). The magnetic susceptibility effects due to the presence of iron in the amyloid plaques near or around the vessels may create signal voids in MRA that may have no connection with flow disturbance (El Tannir El Tayara et al., 2010). However, we did not observe any severe iron deposition in Tg2576 mouse brain (supplementary Fig. S3), thus ruling out the contribution of iron-related susceptibility effects to the signal voids seen in the MRA images for this mouse model.

The frequency and severity of CAA in Tg2576 mice are age related (Domnitz et al., 2005). The CAA first accumulates in the anterior region of the brain in large arteries around the 10th month of age and then progress toward smaller vessels distal from the midline and lateral side of the brain (16 months) and finally at an advanced age of 23 months almost all the vessels are affected by CAA (Domnitz et al., 2005). Our *in vivo* age-dependent MRA studies have shown severe impairment of blood flow starting only at the older age of 18 months, (Figs. 4D and 5C, D) suggesting that after a certain level of elevation of Aβ, cerebrovascular abnormalities can be observed with MRA in these Tg2576 mice. Consistent with this suggestion, extensive loss of vascular smooth cells (VSMCs) correlated with severity of the CAA was reported in older Tg2576 mice (Christie et al., 2001; Han et al., 2008). These results confirmed that mild amounts of CAA have little or no effect on vessel wall integrity. However, as amounts of CAA increase significant disruptions of vessel wall integrity develop, including considerable losses of VSMCs (Han et al., 2008). In addition, a more recent MRA study reported blood flow alterations in the thalamic vessels of APP23 mice and histology results showed capillary CAA association with vessel occlusion and cerebral blood flow disturbances in APP23 mice (Thal et al., 2009). Despite these findings, in another MRA study drastic cerebral blood flow disturbance was observed in APP23 mice brain, which did not correlate with CAA levels, such that deposits of amyloid plaques were not observed in

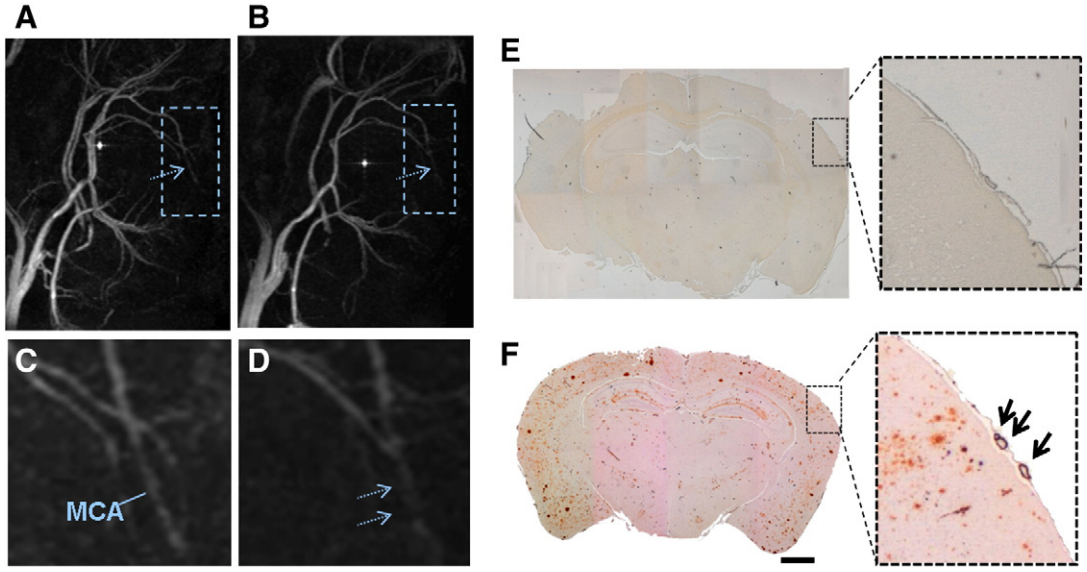

Fig. 6. Angiogram in sagittal view of an 18-month-old wild-type (A) and a Tg2576 mouse (B). The magnified subsampled area of the wild-type mouse shows the visible blood flow signal from branches of MCA (C), however in the Tg2576 mouse a marked decrease in blood flow signal intensity from the branches of the MCA was observed (D). Histological section of the brain of an 18-month-old wild-type (E) and a Tg2576 mouse (F), stained with monoclonal anti-Aβ (6E10) antibodies. CAA was detected in the territory of the pial branches of the MCA of the Tg2576 mouse, as can be clearly seen (arrows) in the magnified subsampled area on the right in (F). Scale bar, 1 mm.

arteries located in the circle of willis (Beckmann et al., 2003). It was suggested that blood flow abnormalities in the brain might have been caused by soluble Aβ in these mice (Beckmann et al., 2003; Burgermeister et al., 2000). Another study has proposed that small amyloid aggregates associated with the microvasculature lead to morphological and architectural alterations of the vasculature before amyloid plaques appear; resulting in altered local blood flow in APP23 mice (Meyer et al., 2008).

Blood flow alterations associated with increased CAA levels are more severe in APP23 mice (Beckmann et al., 2003), compared to the Tg2576 mice (this study). If mainly soluble Aβ in the blood caused severe blood flow alterations in APP23 mice, this effect should have been very drastic in Tg2576 mice, due to the fact that Tg2576 mice have higher levels of soluble Aβ in the blood (Kuo et al., 2000, 2001). It was stressed that the reason for the relatively rare occurrence of CAA in Tg2576 mice and the significant occurrence in APP23 mice can be related with expression levels and genetic background of the transgenic lines (Burgermeister et al., 2000).

Potential causal factors for cerebral blood flow abnormalities observed in our study and other studies may not be limited to Aβ levels (soluble and/or insoluble), but also other factors that are independent of CAA level might have been contributed blood flow abnormalities (Beckmann et al., 2003; El Tannir El Tayara et al., 2010; Shin et al., 2007; Thal et al., 2008). Vascular oxidative stresses have been related to alterations in cerebrovascular dysfunction in AD (Bennett et al., 2009). Superoxide-producing enzyme NADPH oxidase, a major source of reactive oxygen species (ROS), appears to play a central role in cerebrovascular dysfunction (Park et al., 2008). Recently, it has been reported that 12- to 15-month-old Tg2576 mice lacking the catalytic subunit, Nox2, of NADPH oxidase do not develop

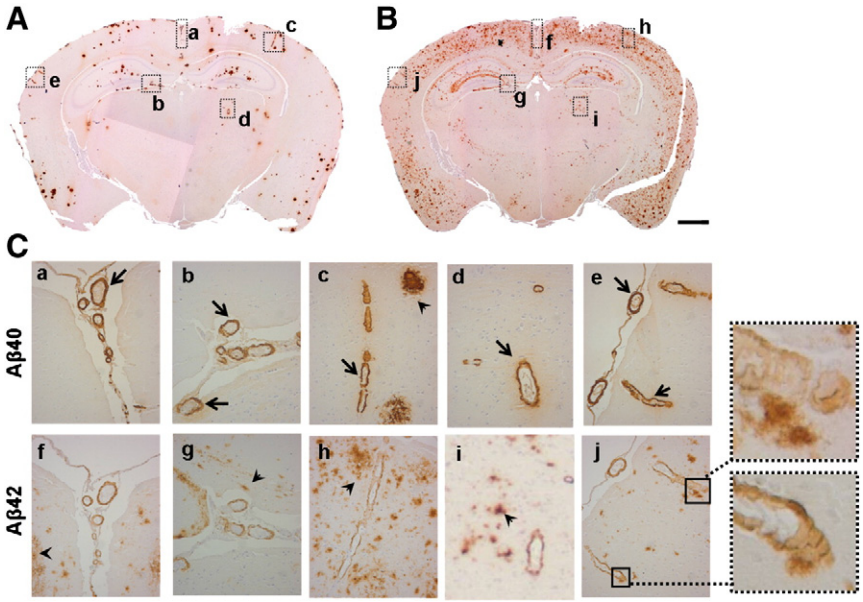

Fig. 7. CAA detected in the brain sections of 23-month-old Tg2576 mouse stained with anti Aβ40 (A) and anti Aβ42 (B). Magnified subsample areas of A (a–e) and B (f–j) are depicted in (C). Aβ-positive plaques in the cortex and hippocampus are shown with arrowheads and CAA affected blood vessels are shown with arrows. Plaques attached to vessels in brain sections stained with Aβ42 are depicted in the enlarged view at the right. Scale bars in A and B, 1 mm.

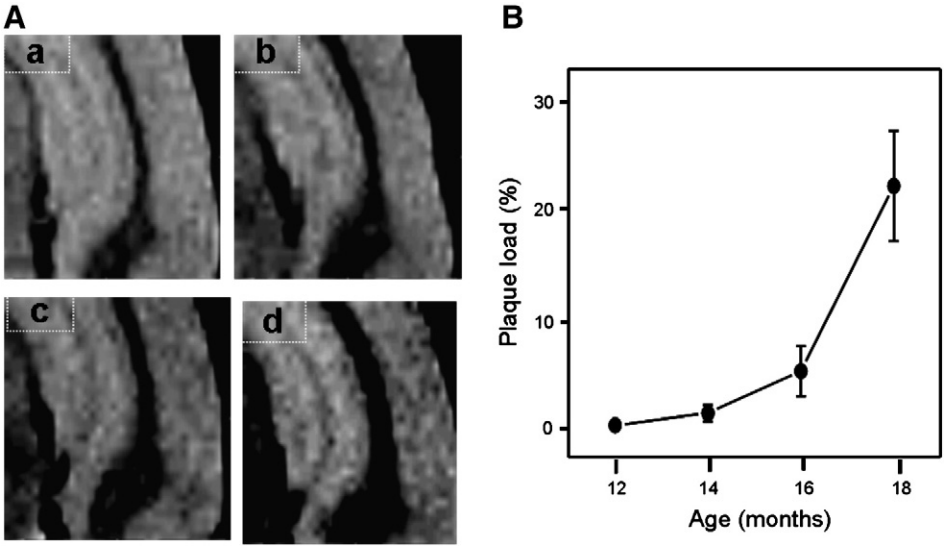

Fig. 8. (A) *In vivo* T2-weighted MR images of the brain of a 16 (a, c) and 23 (b, d) month old control (a, b) and Tg2576 mice (c, d) showing that hypointense regions corresponding to Aβ plaques increased with age in the Tg2576 mouse. (B) Age-dependent changes in Aβ plaques load in a Tg2576 mouse detected by μMRI.

oxidative stress, cerebrovascular dysfunction, or behavioral deficits, suggesting a potential role for ROS in CAA-induced vessel dysfunction (Park et al., 2008). Subsequently it was reported that cerebrovascular dysfunction in aged Tg2576 mice can be fully rescued by antioxidants and the peroxisome proliferator-activated receptor agonist pioglitazone (Nicolakakis et al., 2008). In addition, Aβ induced endothelial dysfunction, which is characterized by impaired endothelium-dependent vasodilation due to an reduced endothelial production of vasodilators, such as nitric oxide (NO) and an increased release of vasoconstrictors including endothelin-1 (ET-1), might be playing a role in cerebral flow abnormalities in AD (Elesber et al., 2006). In spite of this multitude of findings, the causal factors for blood flow abnormalities occurring in vessels of Tg2576 mice and other AD mouse models require further investigation. Being able to follow progression of vascular abnormalities *in vivo* can increase our understanding of such causal factors.

Age-dependent increase in Aβ plaque load

To explore the temporal relationship between *in vivo* plaque load development in the brain tissue and blood flow abnormalities, we performed high-resolution μMRI in parallel to MRA in the same Tg2576 mice with age. Fig. 8A depicts *in vivo* T2-weighted MR images of the brain of a 16 and 23-month-old control and Tg2576 mouse. Hypointense regions corresponding to Aβ plaques were observed in Tg2576 mouse brain and increased with age (Fig. 8A). As expected Aβ plaques were not visible in control mouse brain. The quantitative analysis of Aβ plaque load in cortex in Tg2576 mice between 12 and 18 months of age is shown in Fig. 8B. A marked increase in plaque load was observed in Tg2576 mice with age. However, the increase in plaque load was more rapid between 16 and 18 months of age (Fig. 8B). This time course matches well with the drastic increase in blood flow defect between 16 and 18 months of age seen in same Tg2576 mice (Figs. 4D and 5C, D). These results indicate that severity of amyloid plaque deposition in the brain parenchyma and cerebrovascular deposition of Aβ may be closely linked.

In conclusion, in this study we optimized and performed 3D TOF MRA at 17.6 T for detailed *in vivo* assessment of mouse cerebral vasculature and to compare the age- dependent alteration in cerebral vasculature in control and Tg2576 transgenic mouse models of AD. Our results show that MRA significantly benefits from the ultra-high magnetic field strength (17.6 T) especially to visualize smaller vessels. Age-dependent blood flow abnormalities were observed *in vivo* in MCA and AComA of 18-month-old Tg2576 mice. In addition, histology data showed cerebrovascular amyloid deposition in Tg2576 mice. These results show that vascular abnormalities observed in this study are part of the pathological alterations developed by Tg2576 mouse models of AD. MRA studies at ultra-high magnetic field provide a powerful non-invasive tool to test the effectiveness of putative disease-modifying therapeutic intervention in mouse model of AD *in vivo*.

Acknowledgments

This work was partly supported by grants from Internationale Stichting Alzheimer Onderzoek (ISAO) and Centre for Medical Systems Biology (CMSB). We thank Janneke Ravensbergen, Niels Braakman, Fons Lefeber, Kees Erkelens and S.G. van Duinen for help and useful discussions. The authors like to express their gratitudes to Dr. Karen Hsiao Ashe, Department of Neurology, University of Minnesota, USA, for kindly providing three Tg2576 founder mice.

Appendix A. Supplementary data

Supplementary data to this article can be found online at doi:10.1016/j.neuroimage.2011.12.055.

References

Anderson, C.M., Saloner, D., Tsuruda, J.S., Shapeero, L.G., Lee, R.E., 1990. Artifacts in maximum-intensity-projection display of MR angiograms. AJR Am. J. Roentgenol. 154, 623–629.
Beckmann, N., 2011. Probing cerebrovascular alterations in Alzheimer's disease using MRI: from transgenic models to patients. Curr. Med. Imaging Rev. 7, 51–61.
Beckmann, N., Stirnimann, R., Bochelen, D., 1999. High-resolution magnetic resonance angiography of the mouse brain: application to murine focal cerebral ischemia models. J. Magn. Reson. 140, 442–450.
Beckmann, N., Schuler, A., Mueggler, T., Meyer, E.P., Wiederhold, K.H., Staufenbiel, M., Krucker, T., 2003. Age-dependent cerebrovascular abnormalities and blood flow disturbances in APP23 mice modeling Alzheimer's disease. J. Neurosci. 23, 8453–8459.
Beckmann, N., Gerard, C., Abramowski, D., Cannet, C., Staufenbiel, M., 2011. Noninvasive magnetic resonance imaging detection of cerebral amyloid angiopathy-related microvascular alterations using superparamagnetic iron oxide particles in APP transgenic mouse models of Alzheimer's disease: application to passive Abeta immunotherapy. J. Neurosci. 31, 1023–1031.
Bennett, S., Grant, M.M., Aldred, S., 2009. Oxidative stress in vascular dementia and Alzheimer's disease: a common pathology. J. Alzheimers Dis. 17, 245–257.
Biffi, A., Greenberg, S.M., 2011. Cerebral amyloid angiopathy: a systematic review. J. Clin. Neurol. 7, 1–9.

Braakman, N., Matysik, J., van Duinen, S.G., Verbeek, F., Schliebs, R., de Groot, H.J., Alia, A., 2006. Longitudinal assessment of Alzheimer's beta-amyloid plaque development in transgenic mice monitored by in vivo magnetic resonance microimaging. J. Magn. Reson. Imaging 24, 530–536.

Bürger, S., Noack, M., Kirazov, L.P., Kirazov, E.P., Naydenov, C.L., Kouznetsova, E., Yafai, Y., Schliebs, R., 2009. Vascular endothelial growth factor (VEGF) affects processing of amyloid precursor protein and beta-amyloidogenesis in brain slice cultures derived from transgenic Tg2576 mouse brain. Int. J. Dev. Neurosci. 27, 517–523.

Bürger, S., Yafai, Y., Bigl, M., Wiedemann, P., Schliebs, R., 2010. Effect of VEGF and its receptor antagonist SU-5416, an inhibitor of angiogenesis, on processing of the β-amyloid precursor protein in primary neuronal cells derived from brain tissue of Tg2576 mice. Int. J. Dev. Neurosci. 28, 597–604.

Burgermeister, P., Calhoun, M.E., Winkler, D.T., Jucker, M., 2000. Mechanisms of cerebrovascular amyloid deposition. Lessons from mouse models. Ann. N. Y. Acad. Sci. 903, 307–316.

Christie, R., Yamada, M., Moskowitz, M., Hyman, B., 2001. Structural and functional disruption of vascular smooth muscle cells in a transgenic mouse model of amyloid angiopathy. Am. J. Pathol. 158, 1065–1071.

Domnitz, S.B., Robbins, E.M., Hoang, A.W., Garcia-Alloza, M., Hyman, B.T., Rebeck, G.W., Greenberg, S.M., Bacskai, B.J., Frosch, M.P., 2005. Progression of cerebral amyloid angiopathy in transgenic mouse models of Alzheimer disease. J. Neuropathol. Exp. Neurol. 64, 588–594.

Dorr, A., Sled, J.G., Kabani, N., 2007. Three-dimensional cerebral vasculature of the CBA mouse brain: a magnetic resonance imaging and micro computed tomography study. Neuroimage 35, 1409–1423.

Duyckaerts, C., Potier, M.C., Delatour, B., 2008. Alzheimer disease models and human neuropathology: similarities and differences. Acta Neuropathol. 115, 5–38.

Dydak, U., Schar, M., 2006. MR spectroscopy and spectroscopic imaging: comparing 3.0 T versus 1.5 T. Neuroimaging Clin. N. Am. 16, 269–283.

El Tannir El Tayara, N.T., Delatour, B., Volk, A., Dhenain, M., 2010. Detection of vascular alterations by in vivo magnetic resonance angiography and histology in APP/PS1 mouse model of Alzheimer's disease. MAGMA 23, 53–64.

Elesber, A.A., Bonetti, P.O., Woodrum, J.E., Zhu, X.Y., Lerman, L.O., Younkin, S.G., Lerman, A., 2006. Bosentan preserves endothelial function in mice overexpressing APP. Neurobiol. Aging 27, 446–450.

Ellis, R.J., Olichney, J.M., Thal, L.J., Mirra, S.S., Morris, J.C., Beekly, D., Heyman, A., 1996. Cerebral amyloid angiopathy in the brains of patients with Alzheimer's disease: the CERAD experience, Part XV. Neurology 46, 1592–1596.

Franceschi, M., Alberoni, M., Bressi, S., Canal, N., Comi, G., Fazio, F., Grassi, F., Perani, D., Volonte, M.A., 1995. Correlations between cognitive impairment, middle cerebral artery flow velocity and cortical glucose metabolism in the early phase of Alzheimer's disease. Dementia 6, 32–38.

Fushimi, Y., Miki, Y., Kikuta, K., Okada, T., Kanagaki, M., Yamamoto, A., Nozaki, K., Hashimoto, N., Hanakawa, T., Fukuyama, H., Togashi, K., 2006. Comparison of 3.0- and 1.5-T three-dimensional time-of-flight MR angiography in moyamoya disease: preliminary experience. Radiology 239, 232–237.

Ghiso, J., Frangione, B., 2001. Cerebral amyloidosis, amyloid angiopathy, and their relationship to stroke and dementia. J. Alzheimers Dis. 3, 65–73.

Han, B.H., Zhou, M.L., Abousaleh, F., Brendza, R.P., Dietrich, H.H., Koenigsknecht-Talboo, J., Cirrito, J.R., Milner, E., Holtzman, D.M., Zipfel, G.J., 2008. Cerebrovascular dysfunction in amyloid precursor protein transgenic mice: contribution of soluble and insoluble amyloid-beta peptide, partial restoration via gamma-secretase inhibition. J. Neurosci. 28, 13542–13550.

Harigaya, Y., Tomidokoro, Y., Ikeda, M., Sasaki, A., Kawarabayashi, T., Matsubara, E., Kanai, M., Saido, T.C., Younkin, S.G., Shoji, M., 2006. Type-specific evolution of amyloid plaque and angiopathy in APPsw mice. Neurosci. Lett. 395, 37–41.

Hawkes, C.A., Hartig, W., Kacza, J., Schliebs, R., Weller, R.O., Nicoll, J.A., Carare, R.O., 2011. Perivascular drainage of solutes is impaired in the ageing mouse brain and in the presence of cerebral amyloid angiopathy. Acta Neuropathol. 121, 431–443.

Hennig, J., Nauerth, A., Friedburg, H., 1986. RARE imaging: a fast imaging method for clinical MR. Magn. Reson. Med 3, 823–833.

Herzig, M.C., Winkler, D.T., Burgermeister, P., Pfeifer, M., Kohler, E., Schmidt, S.D., Danner, S., Abramowski, D., Sturchler-Pierrat, C., Burki, K., van Duinen, S.G., Maat-Schieman, M.L., Staufenbiel, M., Mathews, P.M., Jucker, M., 2004. Abeta is targeted to the vasculature in a mouse model of hereditary cerebral hemorrhage with amyloidosis. Nat. Neurosci. 7, 954–960.

Holtzman, D.M., Fagan, A.M., Mackey, B., Tenkova, T., Sartorius, L., Paul, S.M., Bales, K., Ashe, K.H., Irizarry, M.C., Hyman, B.T., 2000. Apolipoprotein E facilitates neuritic and cerebrovascular plaque formation in an Alzheimer's disease model. Ann. Neurol. 47, 739–747.

Howles, G.P., Ghaghada, K.B., Qi, Y., Mukundan Jr., S., Johnson, G.A., 2009. High-resolution magnetic resonance angiography in the mouse using a nanoparticle blood-pool contrast agent. Magn. Reson. Med. 62, 1447–1456.

Hsiao, K., Chapman, P., Nilsen, S., Eckman, C., Harigaya, Y., Younkin, S., Yang, F., Cole, G., 1996. Correlative memory deficits, Abeta elevation, and amyloid plaques in transgenic mice. Science 274, 99–102.

Hu, X., Norris, D.G., 2004. Advances in high-field magnetic resonance imaging. Annu. Rev. Biomed. Eng. 6, 157–184.

Ishibashi, K., Tanaka, K., Nakabayashi, T., Nakamura, M., Uchiyama, M., Okawa, M., 1998. Latent cerebral artery stenoses on magnetic resonance angiography in a patient diagnosed as probable Alzheimer disease. Psychiatry Clin. Neurosci. 52, 93–96.

Kantarci, K., Jack Jr., C.R., 2004. Quantitative magnetic resonance techniques as surrogate markers of Alzheimer's disease. NeuroRx. 1 (2), 196–205.

Kumar-Singh, S., 2008. Cerebral amyloid angiopathy: pathogenetic mechanisms and link to dense amyloid plaques. Genes Brain Behav. 7, 67–82.

Kumar-Singh, S., Pirici, D., McGowan, E., Serneels, S., Ceuterick, C., Hardy, J., Duff, K., Dickson, D., Van Broeckhoven, C., 2005. Dense-core plaques in Tg2576 and PSAPP mouse models of Alzheimer's disease are centered on vessel walls. Am. J. Pathol. 167, 527–543.

Kuo, Y.M., Crawford, F., Mullan, M., Kokjohn, T.A., Emmerling, M.R., Weller, R.O., Roher, A.E., 2000. Elevated A beta and apolipoprotein E in A betaPP transgenic mice and its relationship to amyloid accumulation in Alzheimer's disease. Mol. Med. 6, 430–439.

Kuo, Y.M., Beach, T.G., Sue, L.I., Scott, S., Layne, K.J., Kokjohn, T.A., Kalback, W.M., Luehrs, D.C., Vishnivetskaya, T.A., Abramowski, D., Sturchler-Pierrat, C., Staufenbiel, M., Weller, R.O., Roher, A.E., 2001. The evolution of A beta peptide burden in the APP23 transgenic mice: implications for A beta deposition in Alzheimer disease. Mol. Med. 7, 609–618.

Merlini, M., Meyer, E.P., Ulmann-Schuler, A., Nitsch, R.M., 2011. Vascular beta-amyloid and early astrocyte alterations impair cerebrovascular function and cerebral metabolism in transgenic arcAbeta mice. Acta Neuropathol.. doi:10.1007/s00401-011-0834-y.

Meyer, E.P., Ulmann-Schuler, A., Staufenbiel, M., Krucker, T., 2008. Altered morphology and 3D architecture of brain vasculature in a mouse model for Alzheimer's disease. Proc. Natl. Acad. Sci. U. S. A. 105, 3587–3592.

Nicolakakis, N., Aboulkassim, T., Ongali, B., Lecrux, C., Fernandes, P., Rosa-Neto, P., Tong, X.K., Hamel, E., 2008. Complete rescue of cerebrovascular function in aged Alzheimer's disease transgenic mice by antioxidants and pioglitazone, a peroxisome proliferator-activated receptor gamma agonist. J. Neurosci. 28, 9287–9296.

Nishitsuji, K., Tomiyama, T., Ishibashi, K., Kametani, F., Ozawa, K., Okada, R., Maat-Schieman, M.L., Roos, R.A., Iwai, K., Mori, H., 2007. Cerebral vascular accumulation of Dutch-type Abeta42, but not wild-type Abeta42, in hereditary cerebral hemorrhage with amyloidosis, Dutch type. J. Neurosci. Res. 85, 2917–2923.

Niwa, K., Carlson, G.A., Iadecola, C., 2000. Exogenous A beta1-40 reproduces cerebrovascular alterations resulting from amyloid precursor protein overexpression in mice. J. Cereb. Blood Flow Metab. 20, 1659–1668.

Okuyama, S., Okuyama, J., Tamatsu, Y., Shimada, K., Hoshi, H., Iwai, J., 2004. The arterial circle of Willis of the mouse helps to decipher secrets of cerebral vascular accidents in the human. Med. Hypotheses 63, 997–1009.

Park, L., Zhou, P., Pitstick, R., Capone, C., Anrather, J., Norris, E.H., Younkin, L., Younkin, S., Carlson, G., McEwen, B.S., Iadecola, C., 2008. Nox2-derived radicals contribute to neurovascular and behavioral dysfunction in mice overexpressing the amyloid precursor protein. Proc. Natl. Acad. Sci. U. S. A. 105, 1347–1352.

Pezzini, A., Del Zotto, E., Volonghi, I., Giossi, A., Costa, P., Padovani, A., 2009. Cerebral amyloid angiopathy: a common cause of cerebral hemorrhage. Curr. Med. Chem. 16, 2498–2513.

Pfeifer, L.A., White, L.R., Ross, G.W., Petrovitch, H., Launer, L.J., 2002. Cerebral amyloid angiopathy and cognitive function: the HAAS autopsy study. Neurology 58, 1629–1634.

Poduslo, J.F., Hultman, K.L., Curran, G.L., Preboske, G.M., Chamberlain, R., Marjanska, M., Garwood, M., Jack Jr., C.R., Wengenack, T.M., 2011. Targeting vascular amyloid in arterioles of Alzheimer disease transgenic mice with amyloid beta protein antibody-coated nanoparticles. J. Neuropathol. Exp. Neurol. 70, 653–661.

Reese, T., Bochelen, D., Sauter, A., Beckmann, N., Rudin, M., 1999. Magnetic resonance angiography of the rat cerebrovascular system without the use of contrast agents. NMR Biomed. 12, 189–196.

Revesz, T., Holton, J.L., Lashley, T., Plant, G., Rostagno, A., Ghiso, J., Frangione, B., 2002. Sporadic and familial cerebral amyloid angiopathies. Brain Pathol. 12, 343–357.

Schambach, S.J., Bag, S., Steil, V., Isaza, C., Schilling, L., Groden, C., Brockmann, M.A., 2009. Ultrafast high-resolution in vivo volume-CTA of mice cerebral vessels. Stroke 40, 1444–1450.

Schliebs, R., Arendt, T., 2011. The cholinergic system in aging and neuronal degeneration. Behav. Brain Res. 221, 555–563.

Shin, H.K., Jones, P.B., Garcia-Alloza, M., Borrelli, L., Greenberg, S.M., Bacskai, B.J., Frosch, M.P., Hyman, B.T., Moskowitz, M.A., Ayata, C., 2007. Age-dependent cerebrovascular dysfunction in a transgenic mouse model of cerebral amyloid angiopathy. Brain 130, 2310–2319.

Smith, E.E., Vijayappa, M., Lima, F., Delgado, P., Wendell, L., Rosand, J., Greenberg, S.M., 2008. Impaired visual evoked flow velocity response in cerebral amyloid angiopathy. Neurology 71, 1424–1430.

Thal, D.R., Griffin, W.S., de Vos, R.A., Ghebremedhin, E., 2008. Cerebral amyloid angiopathy and its relationship to Alzheimer's disease. Acta Neuropathol. 115, 599–609.

Thal, D.R., Capetillo-Zarate, E., Larionov, S., Staufenbiel, M., Zurbruegg, S., Beckmann, N., 2009. Capillary cerebral amyloid angiopathy is associated with vessel occlusion and cerebral blood flow disturbances. Neurobiol. Aging 30, 1936–1948.

van de Ven, R.C., Hogers, B., van den Maagdenberg, A.M., de Groot, H.J., Ferrari, M.D., Frants, R.R., Poelmann, R.E., van der Weerd, L., Kiihne, S.R., 2007. T(1) relaxation in in vivo mouse brain at ultra-high field. Magn. Reson. Med. 58, 390–395.

Yamada, M., 2000. Cerebral amyloid angiopathy: an overview. Neuropathology 20, 8–22.

Yamada, M., 2002. Risk factors for cerebral amyloid angiopathy in the elderly. Ann. N. Y. Acad. Sci. 977, 37–44.